

Article

Histidine Functionalized Gold Nanoparticles for Screening Aminoglycosides and Nanomolar Level Detection of Streptomycin in Water, Milk, and Whey

Surendra Krushna Shinde ¹, Dae-Young Kim ¹, Rijuta Ganesh Saratale ², Avinash Ashok Kadam ² , Ganesh Dattatraya Saratale ³ , Asad Syed ⁴, Ali H. Bahkali ⁴ and Gajanan Sampatrao Ghodake ^{1,*} 

¹ Department of Biological and Environmental Science, Dongguk University-Seoul, 32 Dongguk-ro, Ilsandong-gu, Goyang-si 10326, Gyeonggi-do, Korea; shindesurendra9@gmail.com (S.K.S.); sbpkim@dongguk.edu (D.-Y.K.)

² Research Institute of Biotechnology and Medical Converged Science, Dongguk University-Seoul, 32 Dongguk-ro, Ilsandong-gu, Goyang-si 10326, Gyeonggi-do, Korea; rijutaganesh@gmail.com (R.G.S.); avikadam2010@gmail.com (A.A.K.)

³ Department of Food Science and Biotechnology, Dongguk University-Seoul, 32 Dongguk-ro, Ilsandong-gu, Goyang-si 10326, Gyeonggi-do, Korea; gdsaratale@gmail.com

⁴ Department of Botany and Microbiology, College of Science, King Saud University, P.O. Box 2455, Riyadh 11451, Saudi Arabia; asadsayyed@gmail.com (A.S.); abahkali@ksu.edu.sa (A.H.B.)

* Correspondence: ghodakegs@gmail.com; Tel.: +82-31-961-5159; Fax: +82-31-961-5122



Citation: Shinde, S.K.; Kim, D.-Y.; Saratale, R.G.; Kadam, A.A.; Saratale, G.D.; Syed, A.; Bahkali, A.H.; Ghodake, G.S. Histidine Functionalized Gold Nanoparticles for Screening Aminoglycosides and Nanomolar Level Detection of Streptomycin in Water, Milk, and Whey. *Chemosensors* **2021**, *9*, 358. <https://doi.org/10.3390/chemosensors9120358>

Academic Editor: Maria Grzeszczuk

Received: 18 October 2021

Accepted: 12 December 2021

Published: 14 December 2021

Publisher's Note: MDPI stays neutral with regard to jurisdictional claims in published maps and institutional affiliations.



Copyright: © 2021 by the authors. Licensee MDPI, Basel, Switzerland. This article is an open access article distributed under the terms and conditions of the Creative Commons Attribution (CC BY) license (<https://creativecommons.org/licenses/by/4.0/>).

Abstract: Aminoglycoside (AMG) antibiotics are being applied to treat infections caused by Gram-negative bacteria, mainly in livestock, and are prescribed only in severe cases because of their adverse impacts on human health and the environment. Monitoring antibiotic residues in dairy products relies on the accessibility of portable and efficient analytical techniques. Presently, high-throughput screening techniques have been proposed to detect several antimicrobial drugs having identical structural and functional features. The L-histidine functionalized gold nanoparticles (His@AuNPs) do not form a complex with other tested antibiotic classes but show high selectivity for AMG antibiotics. We used ligand-induced aggregation of His@AuNPs as a rapid and sensitive localized surface plasmon resonance (LSPR) assay for AMG antibiotics, producing longitudinal extinction shifts at 660 nm. Herein, we explore the practical application of His@AuNPs to detect streptomycin spiked in water, milk, and whey fraction of milk with nanomolar level sensitivity. The ability of the analytical method to recognize target analytes sensitively and rapidly is of great significance to perform monitoring, thus would certainly reassure widespread use of AMG antibiotics. The biosynthesis of hybrid organic–inorganic metal nanoparticles like His@AuNPs with desired size distribution, stability, and specific host–guest recognition proficiency, would further facilitate applications in various other fields.

Keywords: histidine; gold nanoparticles; aminoglycoside; antibiotics; colorimetric changes; spectral shift; real samples; milk samples; whey fraction

1. Introduction

Antibacterial drugs have been commonly applied as human and veterinary medicine to treat a wide range of infectious diseases [1–3]. Aminoglycosides (AMG) are broad-spectrum antibiotics, are commonly prescribed for humans and a range of livestock, mainly for infections caused by Gram-negative bacteria. Thus, there is an ever-growing concern of direct exposure of residual drugs [4] and adulteration of the food chains [4–6]. Besides this, AMG antibiotics induce adverse effects on human health include allergic reactions [7], cytotoxicity [8,9], nephrotoxicity [10], as well as negative impacts on the environment and risk of antibiotic resistance [11–13]. In this account, we target the development of an

analytical method for ultrasensitive detection of AMG antibiotics commonly found in dairy products and dairy wastewater.

Accompanied by human and livestock health hazards, the residual content of antibacterial drugs in milk is known for their negative impacts on fermentation and cheese production processes [14]. As a result, dairy production industries and quality control departments must screen receiving milk samples and generated wastewater for the residual presence of antibacterial drugs. It is required to protect milk quality, avoid entering antibiotics into the food chain, and prevent direct discharge of contaminated wastewater. Health risks analysis posed from residual content of antibiotics in the foods is practically challenging to estimate; maximal residue limits (MRLs) have been enforced and censored by several national and international regulatory organizations [15]. Because milk is among the most-traded and heavily regulated products for quality assurance standards and food safety thus, it would be desirable if the single analytical method is applicable to detect AMG antibiotics with nanomolar level sensitivity [16,17].

So far, several detection systems have been reported to detect antibiotics, which suggests the urgent need and significance in practical applications [18]. The developed methods are based on different approaches, including inhibition of microbial growth [19,20], toggled RNA aptamers [21], electrochemical RNA aptamer [22], multivalence aptamer probes [23], LSPR-based sensors [17,24], chlorophyll-based fluorescent sensing [25], paper-based fluorescence detector [26], microbial receptor-based assays [27], microfluidic system with fluorometric detection [28], liquid chromatographic assays [29,30] and immunoassays [31]. Some of these methods or assays seem to be laborious and time-consuming and not applicable for processing many samples to be screened for several antibiotics from the same class or different.

Therefore, biospecific interactions-based biosensors received considerable attention since one can use them for rapid detection, high sensitivity, and real-time monitoring relatively with high throughput approach of the assay [32–35]. Metal nanoparticles like AuNPs are an excellent candidate for LSPR sensors because of their sensitive spectral response in response to changes in the local environment of the surfaces [36] and ease of monitoring the color change from their sensitive scattering or absorption [37–40]. The absorbance wavelength at which LSPR occurs is owing to change in size [41–43], shape [44–47], aggregation [48–51], and optical properties of the metal nanoparticles [52,53]. Consequently, LSPR can be specifically used to identify changes in the refractive index of the surrounding medium by monitoring peak wavelength shifts or absorbance intensity changes [54–56]. The detection systems based on the LSPR approach were developed and used to target a specific antimicrobial drug, resulting in visual detection and spectrophotometric assays [24,57–59]. Detection systems based on metallic nanoparticles are of great interest since they led to the rapid development of LSPR technologies [36,60,61]. The LSPR approach proposed in this study delivers the possibility of detecting a group of structurally related targets from the AMG class, allowing the development of the alternative biosensor and relatively robust compared to other methods [62–67].

Applying the LSPR-based biosensor approach, one can perform screening or quantitative measurement of target analytes with high specificity and sensitivity. The specificity results suggest that L-histidine ligands have an excellent binding affinity with AMG antibiotics, and a green synthesis route can readily prepare His@AuNPs. His@AuNPs were highly sensitive to AMG antibiotics enables detection in the nanomolar range. This method was used further to demonstrate the possibility of quantitative streptomycin detection and develop practical applications for complex samples like milk and whey fraction of milk.

2. Experimental Section

2.1. Chemicals

Chloroauric acid (HAuCl_4), amikacin, streptomycin, tetracycline, chlortetracycline, ampicillin, and penicillin G were from Sigma–Aldrich (St. Louis, MO, USA). Metacycline, oxytetracycline, and penicillin V were from Cayman (Ann Arbor, MI, USA). Erythromycin,

gentamicin, kanamycin, azithromycin, and clarithromycin were from the Tokyo Chemical Industry, Tokyo, Japan. Neomycin, tobramycin, and doxycycline from the Alfa Aesar from Middlesex County (Tewksbury, MA, USA). L-histidine amino acid, sodium hydroxide, and sodium chloride were from the Dae Jung Chemicals (Shiheung, Korea).

2.2. Biosynthesis and Characterization of His@AuNPs

The biosynthesis of L-histidine functionalized gold nanoparticles (His@AuNPs) was prepared under safer conditions with minor modification of the previously reported method [68], wherein histidine acts as a natural chloroauric acid-reducing and colloidal stabilizing agent. In brief, 3 mL of L-histidine (25 mM), 2.5 mM of NaOH, and 1 mM of HAuCl₄ were mixed under stirring conditions at ambient temperature (25 °C). NaOH additive was also used in the synthesis to facilitate the biosynthesis of His@AuNPs. The total volume of the synthesis solution was adjusted to 20 mL using distilled water. The red-colored colloidal solution obtained after 72 h incubation at ambient temperature was used for purification by centrifugation (12,000 rpm for 15 min), characterization, and LSPR biosensor development.

UV-vis spectrophotometer (Optizen 2120, Daejeon) equipped with the automatic rotary system having eight cells holder was used to measure absorbance and spectral changes. The cuvettes with 1 cm of path length were used to develop the analytical application of His@AuNPs and UV-vis spectrums measured and analyzed. High-resolution transmission electron microscopy (HR-TEM) was done using Technai G² F20, Ames, IA, USA, to observe the size, shape, and dispersion of His@AuNPs. FT-IR spectra were measured using a Vertex 80 (Bruker, Germany) Fourier transform infrared spectrometer using a potassium bromide pellet method. The absorption spectra were acquired in the range of 4000–600 cm⁻¹ for the pure L-histidine powder and the colloidal His@AuNPs solution. X-ray diffraction (XRD) was used to test the crystalline phases of His@AuNPs on a Rigaku Ultima IV, Japan, using Cu-K α radiation system at 45 kV and 40 mA over two theta ranges from 20° to 80°.

2.3. Effect of Dilution and Ionic Strength on His@AuNPs

To improve the sensitivity, we purified His@AuNPs by centrifugation of His@AuNPs and tested the effect of serial dilution in distilled water [69]. The absorbance and UV-vis spectrums of His@AuNP-2 were measured to reveal the impact of successive dilution on Bandwidth ($\Delta\lambda$) and wavelength (λ_{\max}) after every successive dilution of 0.25 mL of distilled water. Then tested the effect of NaCl concentrations as follows: 300 μ L of His@AuNPs suspension was mixed with distilled water at different concentrations of NaCl (1, 2, 3, 4, 5, and 6 mM). These suspensions were used to measure absorbance at 660 nm. His@AuNPs-NaCl solutions were further used to treat with streptomycin concentration about 4 nM. These samples were again used to measure absorbance 660 nm.

2.4. Selectivity of His@AuNPs

We observed the colorimetric response against several antibiotics from four different classes to examine the selectivity of His@AuNPs. The tetracycline class (tetracycline, doxycycline, and minocycline), macrolides class (azithromycin, erythromycin, and clarithromycin), penicillin class (penicillin G, penicillin V, and ampicillin), AMG class (gentamicin, tobramycin, neomycin, amikacin, kanamycin, and streptomycin) were made with effective concentration about 100 nM with His@AuNPs (0.2 mL) adjusted to 1 mL of the reaction mixture using distilled water. The UV-vis spectrums and color changes were recorded for the antibiotics mentioned above. Moreover, rapid changes in colorimetric and spectrophotometric results observed for His@AuNPs suggest that almost all AMG antibiotics would be targeted.

2.5. Real-Time Response of His@AuNPs

The absorbance of His@AuNPs against streptomycin as a model AMG antibiotic was examined as below: 300 μ L of His@AuNPs samples were mixed to 0.68, 0.66, or 0.64 mL

of distilled water, and absorbance data was measured at 660 nm. Real-time absorbance responses were again tested at three different concentrations of streptomycin (3, 6, and 9 nM) at 660 nm for 25 min at intervals of 1 min. UV-vis spectrums of His@AuNPs treated with streptomycin were monitored for long-term changes for 6 h at intervals of 1 h.

2.6. Sensitivity of His@AuNPs

We then examined the sensitivity of His@AuNPs against streptomycin. His@AuNPs solution of about 300 μ L was used to determine concentrations of streptomycin from 0 to 12 nM in water. The absorbance response (660 nm) increases with an increase in the concentration of streptomycin was plotted. The limit of detection (LOD) (A_{660} nm, $n = 3$) of His@AuNPs solution against streptomycin was estimated using equation $3\sigma/k$, where k is defined as the slope of the calibration plot and σ value from the standard deviation as reported in the previous report [70].

2.7. Practical Application of His@AuNPs

Excessive input of AMG antibiotics in animal husbandry causes adulteration of animal-derived fresh products like milk and several processed dairy products, which acts as metabolic disruptors, affects human health, and poses a risk of antibiotic resistance [71]. We apply the method based on the His@AuNPs to detect streptomycin in milk and whey fraction of milk to explore the practical applications. Streptomycin spiked in milk and whey fraction of milk was determined to validate the relevance of His@AuNPs to monitor real complex samples. Fresh milk samples were procured from the local market, spiked with streptomycin, and processed according to the previous method [72]. In brief, 1% (v/v) trichloroacetic acid was mixed with the milk samples ($n = 3$), and the solution was further sonicated for 20 min to eliminate the protein content from the processed samples. These samples were used to centrifuge at 14,000 rpm for 15 min, and the supernatant fraction was further processed to remove residual lipids using an ultrafiltration membrane (PVDF, 0.22 μ m). The filtrate was used for further storage at 4 $^{\circ}$ C, colorimetric and quantitative detection as mentioned over the range from 1 to 11 nM of streptomycin. Same procedure was performed for whey fraction of milk over the range from 1 to 11 nM of streptomycin.

3. Results and Discussion

3.1. Biosynthesis and Characterization of His@AuNPs

The green synthesis of His@AuNPs was performed; the process seems greatly dependent on the alkaline pH conditions, wherein involves deprotonation of L-histidine functional groups [73,74]. Under the alkaline reaction condition, L-histidine amino acids act as reducing agents and result in stable colloidal suspensions of His@AuNPs, demonstrating simultaneous function as the stabilizing agent. Among other amino acids, histidine is the only amino acid with pKa value near neutrality [75], suitable to stabilize AuNPs at near-neutral and alkaline conditions [76]. The observed results indicate that the functional groups of histidine amino acid, such as α -amino moieties and carboxyl groups, act together to reduce Au ions and form stable electrostatic interactions among AuNPs surfaces [77].

His@AuNPs were further used for the characterization using different techniques, including UV-vis spectrophotometer, FT-IR, XRD, and HR-TEM. Figure 1a shows a sharp and narrow surface plasmon resonance (SPR) band located at 530 nm. The four different XRD diffraction peaks allocated to (111), (200), (220), and (311) planes suggest face-centered cubic structures of His@AuNPs Figure 1b. The XRD profile also shows the peak* is for glass used to prepare the thin film of His@AuNPs using drop casting method. The mean crystallite size of His@AuNPs was estimated using Scherrer equation ($D = K\lambda/(\beta \cos \theta)$) was found about 14 nm \pm 5. HR-TEM imaging was used to observe the size distribution, shape, structure, and dispersion of His@AuNPs. His@AuNPs had narrow size distribution and spherical shape with an average particle size of about 12 nm \pm 6, as shown in the graphical abstract. One can see that His@AuNPs are well dispersed and stable, suggesting a potential candidate for developing analytical applications.

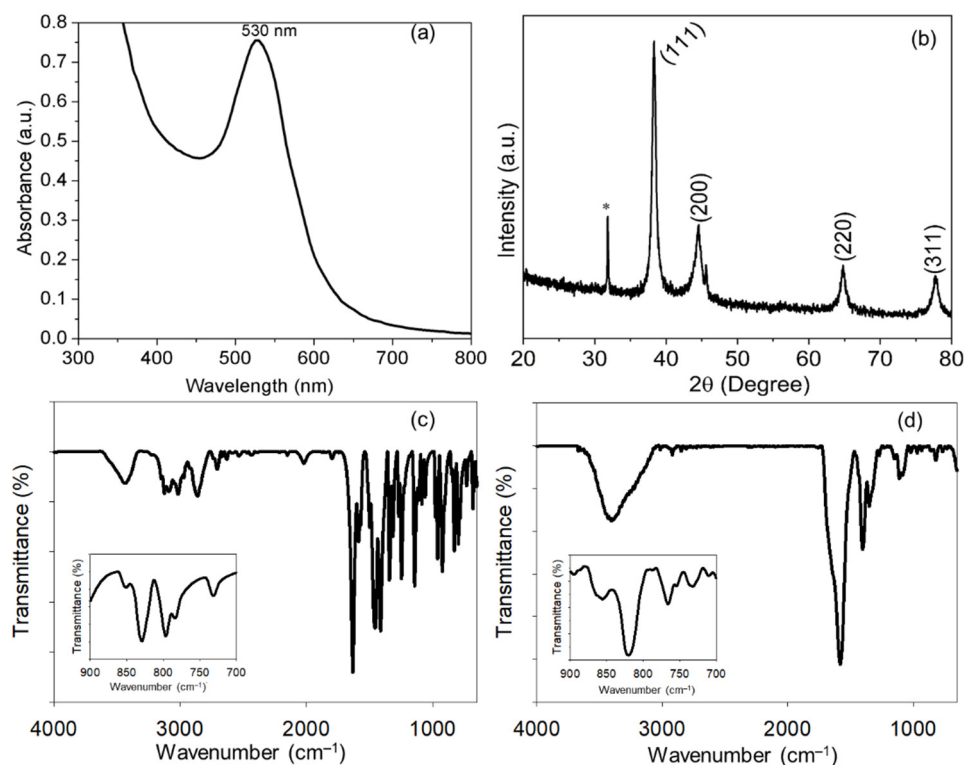


Figure 1. (a) UV-vis spectrum of His@AuNPs, (b) XRD spectrum of His@AuNPs, (c) FT-IR of pure L-histidine, (d) FT-IR of His@AuNPs. The inset shows narrow FT-IR spectra from 700 to 900 cm^{-1} .

The FT-IR spectrum of the pure L-histidine and capped AuNPs shows characteristic vibrational bands, as can be seen in Figure 1c,d. The spectrum for L-histidine shows the peak position at 675–750 cm^{-1} , 1125 cm^{-1} , 1405 cm^{-1} , 1490 cm^{-1} , 1640 cm^{-1} , 2080 cm^{-1} , and 3200–3500 cm^{-1} (Figure 1c) corresponds to bending vibration (δ) of sp^2 CH group, stretching vibration (ν) of CN in imidazole group, symmetric stretching (ν_s) mode of COO^- group, symmetric NH bending, $\nu(\text{C}=\text{C})$, $\nu(\text{N}-\text{H})$, and $\nu(\text{O}-\text{H})$ of H_2O , respectively [77–79]. The binding complex between L-histidine and AuNPs was also studied using FT-IR spectroscopy. The COO^- group allocated at 1405 cm^{-1} for L-histidine found to be shifted to 1385 cm^{-1} for His@AuNPs Figure 1d, specifies interaction of carboxylic group with amine group present in neighbor L-histidine. This result specifies that the binding as well as the complex formation of L-histidine with AuNPs. Figure 1c,d inset shows narrow range IR spectra from 700 to 900 cm^{-1} for free L-histidine and His@AuNPs samples. There is an evident difference at 828 cm^{-1} with a shift of 8 cm^{-1} , for His@AuNPs as compared with the free L-histidine, attributed to $\text{C}_1\text{--C}_2$ stretches along the backbone of L-histidine [76]. The vibrations peak observed at the position 1640 cm^{-1} found shifted to 1600 cm^{-1} and peak followed for pure L-histidine at 1490 cm^{-1} was found absent in His@AuNPs spectra, showing the capping of L-histidine with AuNPs surface via the carboxyl and α -amino moieties binding [77].

3.2. Purification and Stability of His@AuNPs

Excessive Na^+ from NaOH additive and the presence of residual OH^- would cause complications when used for analytical applications. We used centrifugation as a facile purification method, which also allows the removal of unreacted Au ions and uncapped L-histidine molecules [75]. Pellet fraction of His@AuNPs was used to disperse in distilled water and test the impact of successive dilution and ionic strength. The optical properties of His@AuNPs against successive dilution were examined using the measurement of UV-vis spectrophotometer (Figure 2). The plasmon resonance bandwidth ($\Delta\lambda$) and wavelength (λ_{max}) were observed after each dilution by 0.25 mL, used to confirm the excellent stability

of His@AuNPs. UV-vis spectrum is presented in Figure 2a, and their absorbance response observed at 530 nm is plotted against a number of successive dilution cycles Figure 2b. The results were used to select the appropriate volume of His@AuNPs resulting optical density (OD) about 0.2 to 0.3 and used in the LSPR detection system. The α -amino moieties and oxygen of the carboxylic acid functional groups are mainly responsible for the healthy capping and stabilization of AuNPs [76]. The surfaces of His@AuNPs remain negatively charged owing to carboxylate (COO^-) of L-histidine, and the electrostatic repulsion interactions among His@AuNPs enforce long-term stability in neutral to basic conditions [80].

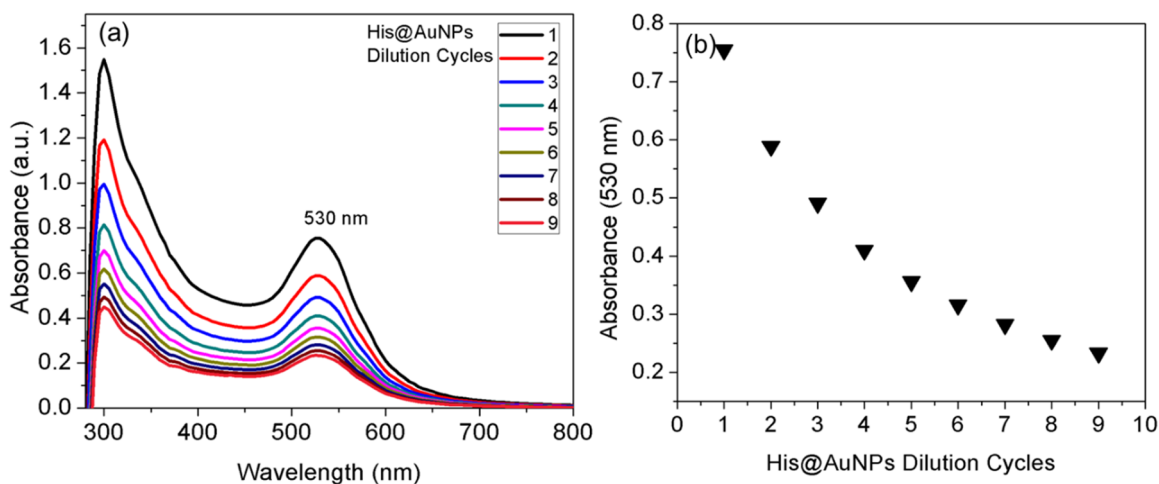


Figure 2. (a) UV-vis spectrum of His@AuNPs recorded after successive dilution with distilled water, (b) Absorbance of His@AuNPs recorded at 530 nm after successive dilution with distilled water.

3.3. Selectivity of His@AuNPs

To assess the selectivity of His@AuNPs, we first observed the colorimetric and spectrophotometric response towards different antibiotics from four different classes, including AMG, tetracycline, macrolide, and penicillin, at a concentration of 100 nM. The specificity of His@AuNPs was examined for other tested antibiotics with identical concentrations and reaction conditions as for AMG antibiotics (Figure 3). Almost all antibiotics selected from the AMG class showed evident colorimetric response from red to blue within a fraction of min; absorbance and spectral change results were then recorded for 25 min (Figure 3a). Our results suggest the coordination of His@AuNPs with AMG class of antibiotics results in apparent amplification of absorbance value observed for 660 nm (Figure 3a). These observations confirm that the plasmon coupling interactions among His@AuNPs occur intensely after the coordination of AMGs [81], resulting in an identical bathochromic shift at 660 nm (Figure 3a). However, antibiotics from other classes cannot cause color change or red-shift or peak broadening, or aggregation of His@AuNPs (Figure 3b–d), thus the possibility of developing a highly selective LSPR biosensor for AMG antibiotics. On this basis, we propose an LSPR biosensor for screening or quantitative detection of AMG antibiotics using His@AuNPs. This novel LSPR biosensor is highly selective towards AMG antibiotics owing to identical structural and functional features.

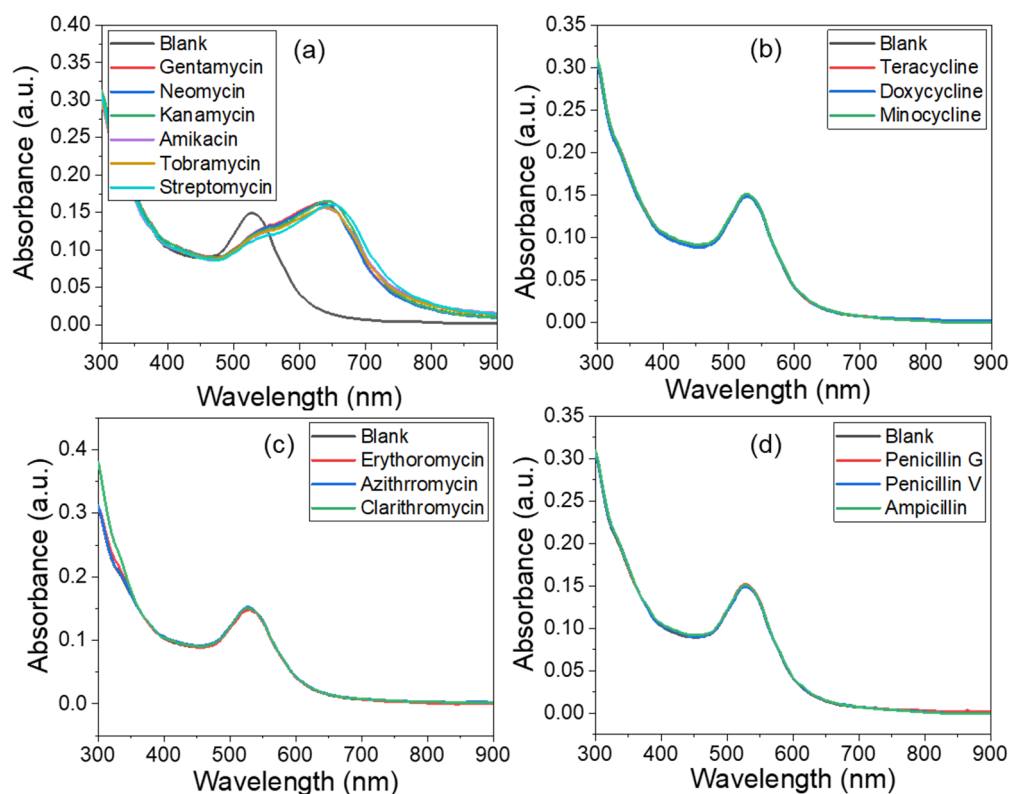


Figure 3. Screening of different antibiotics from four classes: (a) UV-vis spectrum recorded after treatment with AMG class of antibiotics, (b) UV-vis spectrum recorded after treatment with tetracycline class of antibiotics, (c) UV-vis spectrum recorded after treatment with macrolide class of antibiotics, (d) UV-vis spectrum recorded after treatment with penicillin class of antibiotics.

3.4. Sensitivity of His@AuNPs

Then sensitivity of His@AuNPs has been examined towards streptomycin, a model AMG antibiotic in water. Consistent with the increasing concentration of streptomycin, absorbance response at 660 nm and UV-vis spectral shift with broadening towards larger wavelength (660 nm); such peaks emerge quickly and stabilize within 25 min (Figure 4a). The absorbance response was reliant on streptomycin concentration, which was observed identical to the sigmoidal curve (Figure 4b). Concentration-dependent color change from red to blue was also observed with increasing streptomycin of concentration; it can be seen in the inset of Figure 4b. The lowest visual detection concentration by the naked eye is about 4 nM. These results show that His@AuNPs results in a degree of aggregation with the increasing concentration of streptomycin. The absorbance response recorded at 660 nm was found reliant on the concentration of streptomycin; it is used to prepare a calibration plot over a nanomolar range of streptomycin from 0 to 12. His@AuNPs based sensors exhibited a coefficient of determination (R^2) value of about 0.949 and good sensitivity for streptomycin with a LOD of 1.5 nM; the value is competitive compared to other reported methods [21,82,83]. These results suggest that His@AuNPs can develop practical applications for screening residual content or quantifying specific AMG antibiotics in water samples.

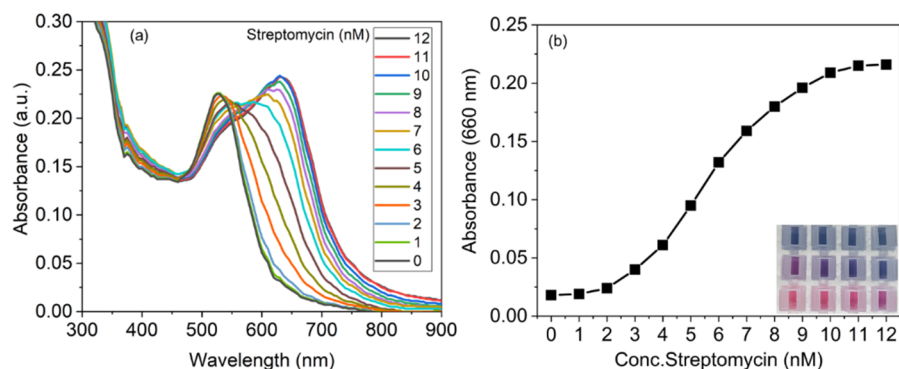


Figure 4. (a) UV-vis spectral response of His@AuNPs in the response of increasing concentration of streptomycin in water, (b) A sigmoidal curve of absorbance intensity at 660 nm vs. streptomycin concentration in nanomolar range.

3.5. Effect of Ionic Strength and Real-Time Response

Investigating the effect of ionic strength is an essential parameter to improve sensitivity against target analyte [84]. The absorbance response of His@AuNPs at different concentrations of NaCl from 1 to 6 mM is presented in Figure 5a. The absorbance intensity recorded at 660 nm seems dependent on ionic strength, tested in the presence of streptomycin 4 nM. The addition of streptomycin to His@AuNPs solution treated with the increasing NaCl concentration indicates the possibility of enhancing the sensitivity of His@AuNPs. As a cationic antibiotic, streptomycin strongly interacts with His@AuNPs. It forms unstable histidine complexes with streptomycin ligands with potential binding sites: carboxyls, amino group, or the imidazole side chain. His@AuNPs surface charge is a negative result from carboxyl functional groups. Therefore, the presence of NaCl even at low concentrations in the His@AuNPs suspensions and then interaction with streptomycin promotes the formation of large aggregates.

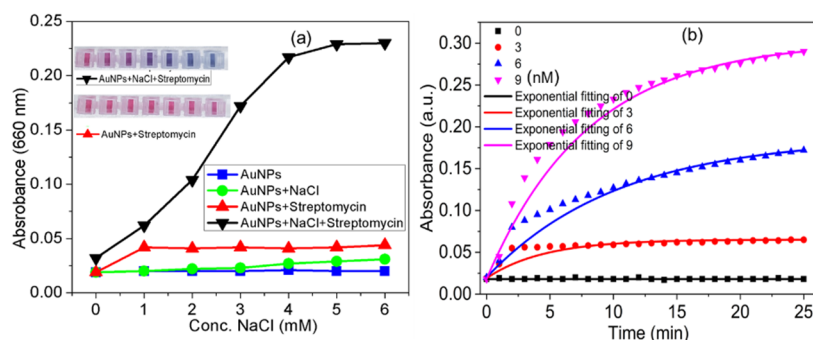


Figure 5. (a) The absorbance response of His@AuNPs against increasing concentration of NaCl recorded at 660 nm in the presence and absence of the streptomycin, (b) The real-time course of the absorbance intensity of His@AuNPs recorded at 660 nm in the presence of the streptomycin concentration (0, 3, 6, 9 nM) with 1 min interval for 25 min.

The real-time absorbance response of His@AuNPs for 660 nm at 1 min interval for 25 min is presented in Figure 5b. The absorbance intensity increases as a function of time and streptomycin concentration. Exponential fitting of real-time absorbance response as a function of time for the His@AuNPs sensor is also presented. Furthermore, time-dependent absorbance growth curves of the His@AuNPs at 660 nm after adding streptomycin (3, 6, and 9 nM) can be well fitted using exponential fitting (Figure 5b). These results indicate the long response time of the His@AuNPs for streptomycin with a likely rapid detection platform. The absorbance intensity (660 nm) increases exponentially up to 10 to 15 min and stabilizes within 20 to 25 min, indicating fractal growth of His@AuNP aggregates, and results found in agreement with a previous report [85].

This detection system responds within a fraction of min; however, it establishes a stable response within 25 min. We chose 25 min as the incubation time for further LSPR measurements performed for streptomycin. His@AuNPs based detection system combined with UV-vis plate reader would be a potential candidate to develop a rapid, point-of-care, portable, and user-friendly analytical platform to target detection of multiple AMG antibiotics.

Most of the colorimetric methods report the color and spectral changes in response to the target analyte. Herein, the temporal evolution of UV-vis spectrums was also investigated to reveal the fate of His@AuNP aggregates. It was readily observed by measuring UV-vis spectrums of His@AuNPs against four different streptomycin concentrations (3, 6, 9, and 12 nM) within the time frame of 1 to 6 h (Figure 6a–d). The longitudinal band owing to red-shift initiates apparently but stabilizes within 6 h for streptomycin (3 nM), indicating fractal growth pattern for His@AuNP aggregates (Figure 6a). Similarly, significant growth of His@AuNP aggregates found within 1 h, stabilizes within 6 h for streptomycin (6 nM) (Figure 6b). His@AuNPs aggregates were found to increase significantly within 1 h for streptomycin (9 nM); then, they remain stable, as seen in Figure 6c. However, His@AuNPs absorbance was found to increase to maximum within 1 h for streptomycin (12 nM), and consistently cause a decrease in absorbance at 660 nm indicates sedimentation of aggregates (Figure 6d). Thus, the growth of His@AuNPs aggregates attributes to the streptomycin concentration, such changes can be readily monitored using UV-vis spectrophotometer [70].

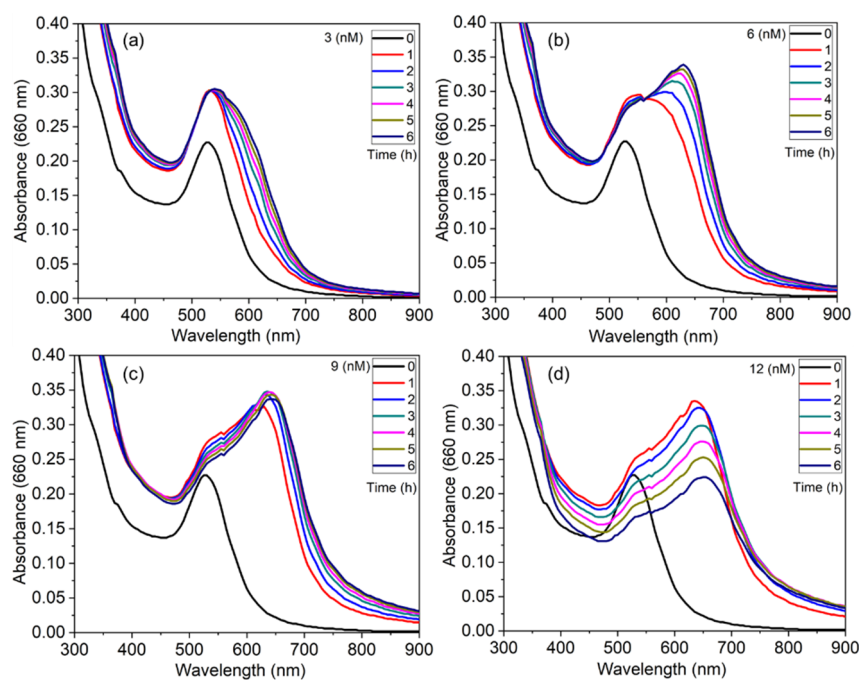


Figure 6. The temporal evolution of UV-vis spectrums of His@AuNPs (a) in the presence of the streptomycin (3 nM); (b) in the presence of the streptomycin (6 nM), (c) in the presence of the streptomycin (9 nM); (d) in the presence of the streptomycin (12 nM).

3.6. Applicability of the Detection System

Contaminated dairy products with AMG antibiotics are of health concern [86–89], which attracted public attention from different parts of the world [90,91]. We apply our method to detect streptomycin spiked milk samples to assess the practical applicability of His@AuNPs. Streptomycin spiked milk samples were prepared by separating proteins and fat content and used for detection visually and quantitatively (Figure 7). The absorbance response increases with an increase in the concentration of streptomycin, along with the emergence of visible red-shift at 660 nm (Figure 7a). The absorbance response seems dependent on the streptomycin concentration (Figure 7b). The absorbance data was used

to prepare a calibration plot for spiked streptomycin over a range of 1 to 11 nM. The visual detection limit for streptomycin spiked milk samples is approximately 3 nM, which can be seen in the inset of Figure 7b. R^2 value found at about 0.974 with a detection limit of about 1.17 nM, considerably lower than the other methods [21,82].

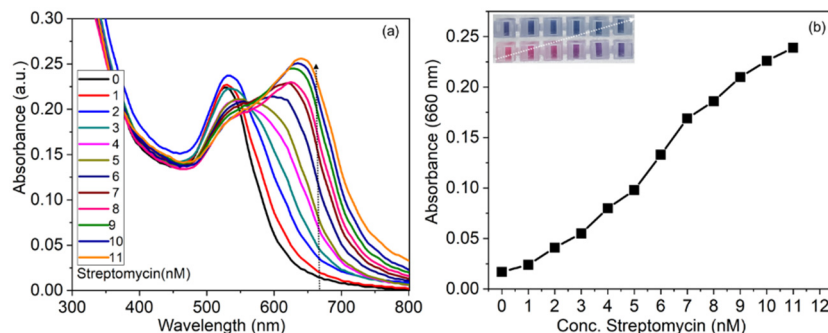


Figure 7. (a) UV-vis spectral response of His@AuNPs in the response of increasing concentration of streptomycin in milk, (b) a calibration curve of absorbance intensity at 660 nm vs. streptomycin concentration in nanomolar.

We further applied our method to detect spiked whey fractions of milk. The absorbance response, spectral changes, and broadening of the peak indicated the formation of visible red-shift towards a larger wavelength (660 nm) (Figure 8a). The absorbance response for the whey fraction of milk was recorded at 660 nm as a function of streptomycin concentration from 1 to 11 nM and plotted in Figure 8b, therefore suggesting that the dependence of the behavior of the probe upon the antibiotic concentration is the same also in whey fraction of milk. The His@AuNPs solution turns red to blue as a response to the increased streptomycin concentration; naked eyes can visually detect up to nanomolar level. The visual detection limit for streptomycin in the whey fraction of milk is about 3 nM, as can be seen in the inset of Figure 8b. The estimated R^2 value was about 0.952 with a detection limit as low as 2.25 nM, which seems much lower than the other conventional analytical methods [82] and MRL values of AMG antibiotics [21]. These results validate further applications of His@AuNPs in monitoring whey wastewater. However, additional efforts are needed to improve the overall efficiency of the detection system, including the design of similar ligands on metal nanoparticles selective for AMG antibiotics, which may contribute to the development of point-of-care services and onsite applications in rural settings.

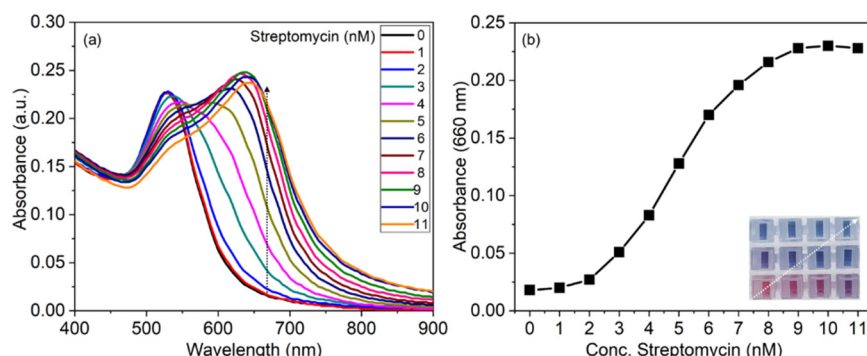


Figure 8. (a) UV-vis spectral response of His@AuNPs in the response of increasing concentration of streptomycin in the whey fraction of milk, (b) a sigmoidal curve of absorbance intensity at 660 nm vs. streptomycin concentration range in nanomolar.

4. Conclusions

In summary, this account presents biosynthesis and characterization of L-histidine functionalized AuNPs and applies for visual and quantitative detection of AMG antibiotics.

Recognition mechanisms like host–guest functionality of L-histidine ligands, the degree of His@AuNPs aggregation controlled by increasing concentration of cationic guest like AMG antibiotics with a high positive charge, convey consistent changes in visible color and LSPR signal. We showed the possibility of implementing an LSPR-based biosensor for quantitative measurements of streptomycin as a model AMG antibiotic residues present in the complex samples like milk and whey fraction of milk. A nanomolar level detection limit for validating our method has practical relevance as it is appropriate to perform quality control and ensure maximal residue limits. Ease of synthesis and capping L-histidine ligands with the AuNPs suggests the possibility of developing other analytical applications using such material and approach.

Author Contributions: Conceptualization, D.-Y.K.; software, A.S.; supervision, A.S. and A.H.B.; validation, G.D.S. and A.H.B.; visualization, G.D.S.; writing—original draft, G.S.G. and S.K.S.; writing—review and editing, R.G.S., and A.A.K. All authors have read and agreed to the published version of the manuscript.

Funding: Researchers Supporting Project number (RSP-2021/15), King Saud University, Riyadh, Saudi Arabia.

Institutional Review Board Statement: Not applicable.

Informed Consent Statement: Informed consent was obtained from all subjects involved in the study.

Data Availability Statement: Not applicable.

Acknowledgments: The authors appreciate Dongguk University-Seoul, South Korea, supporting research (2020–2021). The authors extend their appreciation to the Researchers Supporting Project number (RSP-2021/15), King Saud University, Riyadh, Saudi Arabia.

Conflicts of Interest: The authors confirm no conflict of interest to declare.

References

1. Eibl, C.; Bexiga, R.; Viora, L.; Guyot, H.; Félix, J.; Wilms, J.; Tichy, A.; Hund, A. The Antibiotic Treatment of Calf Diarrhea in Four European Countries: A Survey. *Antibiotics* **2021**, *10*, 910. [[CrossRef](#)] [[PubMed](#)]
2. Little, S.; Woodward, A.; Browning, G.; Billman-Jacobe, H. In-Water Antibiotic Dosing Practices on Pig Farms. *Antibiotics* **2021**, *10*, 169. [[CrossRef](#)]
3. De Briyne, N.; Atkinson, J.; Pokludová, L.; Borriello, S.P. Antibiotics used most commonly to treat animals in Europe. *Vet. Rec.* **2014**, *175*, 325. [[CrossRef](#)]
4. Almeida, M.P.; Rezende, C.P.; Souza, L.F.; Brito, R.B. Validation of a quantitative and confirmatory method for residue analysis of aminoglycoside antibiotics in poultry, bovine, equine and swine kidney through liquid chromatography-tandem mass spectrometry. *Food Addit. Contam. Part A* **2012**, *29*, 517–525. [[CrossRef](#)] [[PubMed](#)]
5. Caglayan, M.O. Aptamer-based ellipsometric sensor for ultrasensitive determination of aminoglycoside group antibiotics from dairy products. *J. Sci. Food Agric.* **2020**, *100*, 3386–3393. [[CrossRef](#)]
6. Tan, X.; Jiang, Y.-W.; Huang, Y.-J.; Hu, S.-H. Persistence of gentamicin residues in milk after the intramammary treatment of lactating cows for mastitis. *J. Zhejiang Univ. Sci. B* **2009**, *10*, 280–284. [[CrossRef](#)] [[PubMed](#)]
7. Childs-Kean, L.M.; Shaer, K.M.; Varghese Gupta, S.; Cho, J.C. Aminoglycoside Allergic Reactions. *Pharmacy* **2019**, *7*, 124. [[CrossRef](#)] [[PubMed](#)]
8. Peloquin, C.A.; Berning, S.E.; Nitta, A.T.; Simone, P.M.; Goble, M.; Huitt, G.A.; Iseman, M.D.; Cook, J.L.; Curran-Everett, D. Aminoglycoside Toxicity: Daily versus Thrice-Weekly Dosing for Treatment of Mycobacterial Diseases. *Clin. Infect. Dis.* **2004**, *38*, 1538–1544. [[CrossRef](#)] [[PubMed](#)]
9. Karasawa, T.; Steyger, P.S. Intracellular mechanisms of aminoglycoside-induced cytotoxicity. *Integr. Biol.* **2011**, *3*, 879–886. [[CrossRef](#)]
10. Swan, S.K. Aminoglycoside nephrotoxicity. *Semin. Nephrol.* **1997**, *17*, 27–33.
11. Zuo, P.; Yu, P.; Alvarez, P.J.J.; Dozois, C.M. Aminoglycosides Antagonize Bacteriophage Proliferation, Attenuating Phage Suppression of Bacterial Growth, Biofilm Formation, and Antibiotic Resistance. *Appl. Environ. Microbiol.* **2021**, *87*. [[CrossRef](#)] [[PubMed](#)]
12. Obayiuwana, A.; Ibekwe, A.M. Antibiotic Resistance Genes Occurrence in Wastewaters from Selected Pharmaceutical Facilities in Nigeria. *Water* **2020**, *12*, 1897. [[CrossRef](#)]
13. Garneau-Tsodikova, S.; Labby, K.J. Mechanisms of Resistance to Aminoglycoside Antibiotics: Overview and Perspectives. *MedChemComm* **2016**, *7*, 11–27. [[CrossRef](#)]

14. Li, J.H.; Yousif, M.H.; Li, Z.Q.; Wu, Z.H.; Li, S.L.; Yang, H.J.; Wang, Y.J.; Cao, Z.J. Effects of antibiotic residues in milk on growth, ruminal fermentation, and microbial community of preweaning dairy calves. *J. Dairy Sci.* **2019**, *102*, 2298–2307. [[CrossRef](#)] [[PubMed](#)]
15. Woodward, K.N. Antibiotics and Drugs | Uses in Food Production. In *Encyclopedia of Food Sciences and Nutrition*, 2nd ed.; Caballero, B., Ed.; Academic Press: Oxford, MS, USA, 2003; pp. 249–254.
16. Kim, S.; Lee, H.J. Gold Nanostar Enhanced Surface Plasmon Resonance Detection of an Antibiotic at Attomolar Concentrations via an Aptamer-Antibody Sandwich Assay. *Anal. Chem.* **2017**, *89*, 6624–6630. [[CrossRef](#)] [[PubMed](#)]
17. Cappi, G.; Spiga, F.M.; Moncada, Y.; Ferretti, A.; Beyeler, M.; Bianchessi, M.; Decosterd, L.; Buclin, T.; Guiducci, C. Label-Free Detection of Tobramycin in Serum by Transmission-Localized Surface Plasmon Resonance. *Anal. Chem.* **2015**, *87*, 5278–5285. [[CrossRef](#)]
18. McKeating, K.S.; Couture, M.; Dinel, M.-P.; Garneau-Tsodikova, S.; Masson, J.-F. High throughput LSPR and SERS analysis of aminoglycoside antibiotics. *Analyst* **2016**, *141*, 5120–5126. [[CrossRef](#)]
19. Gfeller, K.Y.; Nugaeva, N.; Hegner, M. Rapid biosensor for detection of antibiotic-selective growth of *Escherichia coli*. *Appl. Environ. Microbiol.* **2005**, *71*, 2626–2631. [[CrossRef](#)] [[PubMed](#)]
20. Jain, M.C.; Nadaraja, A.V.; Narang, R.; Zarifi, M.H. Rapid and real-time monitoring of bacterial growth against antibiotics in solid growth medium using a contactless planar microwave resonator sensor. *Sci. Rep.* **2021**, *11*, 14775. [[CrossRef](#)]
21. Derbyshire, N.; White, S.J.; Bunka, D.H.J.; Song, L.; Stead, S.; Tarbin, J.; Sharman, M.; Zhou, D.; Stockley, P.G. Toggled RNA Aptamers Against Aminoglycosides Allowing Facile Detection of Antibiotics Using Gold Nanoparticle Assays. *Anal. Chem.* **2012**, *84*, 6595–6602. [[CrossRef](#)]
22. Schoukroun-Barnes, L.R.; Wagan, S.; White, R.J. Correction to Enhancing the Analytical Performance of Electrochemical RNA Aptamer-Based Sensors for Sensitive Detection of Aminoglycoside Antibiotics. *Anal. Chem.* **2014**, *86*, 5188. [[CrossRef](#)]
23. Zhang, Y.; Hu, Y.; Deng, S.; Yuan, Z.; Li, C.; Lu, Y.; He, Q.; Zhou, M.; Deng, R. Engineering Multivalence Aptamer Probes for Amplified and Label-Free Detection of Antibiotics in Aquatic Products. *J. Agric. Food Chem.* **2020**, *68*, 2554–2561. [[CrossRef](#)] [[PubMed](#)]
24. Frasconi, M.; Tel-Vered, R.; Riskin, M.; Willner, I. Surface Plasmon Resonance Analysis of Antibiotics Using Imprinted Boronic Acid-Functionalized Au Nanoparticle Composites. *Anal. Chem.* **2010**, *82*, 2512–2519. [[CrossRef](#)] [[PubMed](#)]
25. Zakharenkova, S.A.; Dobrovolskii, A.A.; Garshev, A.V.; Statkus, M.A.; Beklemishev, M.K. Chlorophyll-Based Self-Assembled Nanostructures for Fluorescent Sensing of Aminoglycoside Antibiotics. *ACS Sustain. Chem. Eng.* **2021**, *9*, 3408–3415. [[CrossRef](#)]
26. Wang, L.; Zhu, F.; Zhu, Y.; Xie, S.; Chen, M.; Xiong, Y.; Liu, Q.; Yang, H.; Chen, X. Intelligent Platform for Simultaneous Detection of Multiple Aminoglycosides Based on a Ratiometric Paper-Based Device with Digital Fluorescence Detector Readout. *ACS Sens.* **2019**, *4*, 3283–3290. [[CrossRef](#)]
27. Ahmed, S.; Ning, J.; Cheng, G.; Ahmad, I.; Li, J.; Mingyue, L.; Qu, W.; Iqbal, M.; Shabbir, M.A.B.; Yuan, Z. Receptor-based screening assays for the detection of antibiotic residues—A review. *Talanta* **2017**, *166*, 176–186. [[CrossRef](#)]
28. Ęcija-Arenas, Á.; Román-Pizarro, V.; Fernández-Romero, J.M. Usefulness of Hybrid Magnetoliposomes for Aminoglycoside Antibiotic Residues Determination in Food Using an Integrated Microfluidic System with Fluorometric Detection. *J. Agric. Food Chem.* **2021**, *69*, 6888–6896. [[CrossRef](#)] [[PubMed](#)]
29. Bobbitt, D.R.; Ng, K.W. Chromatographic analysis of antibiotic materials in food. *J. Chromatogr.* **1992**, *624*, 153–170. [[CrossRef](#)]
30. Liu, Q.; Li, J.; Song, X.; Zhang, M.; Li, E.; Gao, F.; He, L. Simultaneous determination of aminoglycoside antibiotics in feeds using high performance liquid chromatography with evaporative light scattering detection. *RSC Adv.* **2017**, *7*, 1251–1259. [[CrossRef](#)]
31. Ahmed, S.; Ning, J.; Peng, D.; Chen, T.; Ahmad, I.; Ali, A.; Lei, Z.; Abu bakr Shabbir, M.; Cheng, G.; Yuan, Z. Current advances in immunoassays for the detection of antibiotics residues: A review. *Food Agric. Immunol.* **2020**, *31*, 268–290. [[CrossRef](#)]
32. Jung, S.; Kaar, J.L.; Stoykovich, M.P. Design and functionalization of responsive hydrogels for photonic crystal biosensors. *Mol. Syst. Des. Eng.* **2016**, *1*, 225–241. [[CrossRef](#)]
33. Feriotto, G.; Corradini, R.; Sforza, S.; Bianchi, N.; Mischiati, C.; Marchelli, R.; Gambari, R. Peptide Nucleic Acids and Biosensor Technology for Real-Time Detection of the Cystic Fibrosis W1282X Mutation by Surface Plasmon Resonance. *Lab. Investig.* **2001**, *81*, 1415–1427. [[CrossRef](#)]
34. Vello, T.P.; da Silva, L.M.B.; Silva, G.O.; de Camargo, D.H.S.; Corrêa, C.C.; Bof Bufon, C.C. Hybrid organic/inorganic interfaces as reversible label-free platform for direct monitoring of biochemical interactions. *Biosens. Bioelectron.* **2017**, *87*, 209–215. [[CrossRef](#)]
35. Kim, H.-M.; Park, J.-H.; Jeong, D.H.; Lee, H.-Y.; Lee, S.-K. Real-time detection of prostate-specific antigens using a highly reliable fiber-optic localized surface plasmon resonance sensor combined with micro fluidic channel. *Sens. Actuators B Chem.* **2018**, *273*, 891–898. [[CrossRef](#)]
36. Yang, S.; Wu, T.; Zhao, X.; Li, X.; Tan, W. The Optical Property of Core-Shell Nanosensors and Detection of Atrazine Based on Localized Surface Plasmon Resonance (LSPR) Sensing. *Sensors* **2014**, *14*, 13273–13284. [[CrossRef](#)] [[PubMed](#)]
37. Homola, J. Present and future of surface plasmon resonance biosensors. *Anal. Bioanal. Chem.* **2003**, *377*, 528–539. [[CrossRef](#)]
38. Jain, P.K.; El-Sayed, M.A. Plasmonic coupling in noble metal nanostructures. *Chem. Phys. Lett.* **2010**, *487*, 153–164. [[CrossRef](#)]
39. Langer, J.; Novikov, S.M.; Liz-Marzán, L.M. Sensing using plasmonic nanostructures and nanoparticles. *Nanotechnology* **2015**, *26*, 322001. [[CrossRef](#)]
40. Willets, K.A.; Duyne, R.P.V. Localized Surface Plasmon Resonance Spectroscopy and Sensing. *Annu. Rev. Phys. Chem.* **2007**, *58*, 267–297. [[CrossRef](#)] [[PubMed](#)]

41. Lee, T.-H.; Lee, S.-W.; Jung, J.-A.; Ahn, J.; Kim, M.-G.; Shin, Y.-B. Signal Amplification by Enzymatic Reaction in an Immunosensor Based on Localized Surface Plasmon Resonance (LSPR). *Sensors* **2010**, *10*, 2045–2053. [[CrossRef](#)]
42. Hu, Y.; Song, Y.; Wang, Y.; Di, J. Electrochemical synthesis of gold nanoparticles onto indium tin oxide glass and application in biosensors. *Thin Solid Films* **2011**, *519*, 6605–6609. [[CrossRef](#)]
43. Tu, M.H.; Sun, T.; Grattan, K.T.V. LSPR optical fibre sensors based on hollow gold nanostructures. *Sens. Actuators B Chem.* **2014**, *191*, 37–44. [[CrossRef](#)]
44. Chen, H.; Kou, X.; Yang, Z.; Ni, W.; Wang, J. Shape- and Size-Dependent Refractive Index Sensitivity of Gold Nanoparticles. *Langmuir* **2008**, *24*, 5233–5237. [[CrossRef](#)] [[PubMed](#)]
45. Cao, J.; Sun, T.; Grattan, K.T.V. Gold nanorod-based localized surface plasmon resonance biosensors: A review. *Sens. Actuators B Chem.* **2014**, *195*, 332–351. [[CrossRef](#)]
46. Deng, J.; Song, Y.; Wang, Y.; Di, J. Label-free optical biosensor based on localized surface plasmon resonance of twin-linked gold nanoparticles electrodeposited on ITO glass. *Biosens. Bioelectron.* **2010**, *26*, 615–619. [[CrossRef](#)] [[PubMed](#)]
47. Jain, P.K.; Lee, K.S.; El-Sayed, I.H.; El-Sayed, M.A. Calculated Absorption and Scattering Properties of Gold Nanoparticles of Different Size, Shape, and Composition: Applications in Biological Imaging and Biomedicine. *J. Phys. Chem. B* **2006**, *110*, 7238–7248. [[CrossRef](#)]
48. Do, P.Q.T.; Huong, V.T.; Phuong, N.T.T.; Nguyen, T.-H.; Ta, H.K.T.; Ju, H.; Phan, T.B.; Phung, V.-D.; Trinh, K.T.L.; Tran, N.H.T. The highly sensitive determination of serotonin by using gold nanoparticles (Au NPs) with a localized surface plasmon resonance (LSPR) absorption wavelength in the visible region. *RSC Adv.* **2020**, *10*, 30858–30869. [[CrossRef](#)]
49. Liu, B.; Huang, R.; Yu, Y.; Su, R.; Qi, W.; He, Z. Gold Nanoparticle-Aptamer-Based LSPR Sensing of Ochratoxin A at a Widened Detection Range by Double Calibration Curve Method. *Front. Chem.* **2018**, *6*, 94. [[CrossRef](#)]
50. Iarossi, M.; Schiattarella, C.; Rea, I.; De Stefano, L.; Fittipaldi, R.; Vecchione, A.; Velotta, R.; Ventura, B.D. Colorimetric Immunosensor by Aggregation of Photochemically Functionalized Gold Nanoparticles. *ACS Omega* **2018**, *3*, 3805–3812. [[CrossRef](#)]
51. Guo, L.; Xu, Y.; Ferhan, A.R.; Chen, G.; Kim, D.-H. Oriented Gold Nanoparticle Aggregation for Colorimetric Sensors with Surprisingly High Analytical Figures of Merit. *J. Am. Chem. Soc.* **2013**, *135*, 12338–12345. [[CrossRef](#)]
52. Mahmood, H.Z.; Jilani, A.; Farooq, S.; Javed, Y.; Jamil, Y.; Iqbal, J.; Ullah, S.; Wageh, S. Plasmon-Based Label-Free Biosensor Using Gold Nanosphere for Dengue Detection. *Crystals* **2021**, *11*, 1340. [[CrossRef](#)]
53. Gong, X.; Tang, J.; Ji, Y.; Wu, B.; Wu, H.; Liu, A. Adjustable plasmonic optical properties of hollow gold nanospheres monolayers and LSPR-dependent surface-enhanced Raman scattering of hollow gold nanosphere/graphene oxide hybrids. *RSC Adv.* **2015**, *5*, 42653–42662. [[CrossRef](#)]
54. Chen, J.; Shi, S.; Su, R.; Qi, W.; Huang, R.; Wang, M.; Wang, L.; He, Z. Optimization and Application of Reflective LSPR Optical Fiber Biosensors Based on Silver Nanoparticles. *Sensors* **2015**, *15*, 12205–12217. [[CrossRef](#)]
55. Sepúlveda, B.; Angelomé, P.C.; Lechuga, L.M.; Liz-Marzán, L.M. LSPR-based nanobiosensors. *Nano Today* **2009**, *4*, 244–251. [[CrossRef](#)]
56. Shen, Y.; Zhou, J.; Liu, T.; Tao, Y.; Jiang, R.; Liu, M.; Xiao, G.; Zhu, J.; Zhou, Z.K.; Wang, X.; et al. Plasmonic gold mushroom arrays with refractive index sensing figures of merit approaching the theoretical limit. *Nat. Commun.* **2013**, *4*, 2381. [[CrossRef](#)]
57. Reder-Christ, K.; Bendas, G. Biosensor Applications in the Field of Antibiotic Research—A Review of Recent Developments. *Sensors* **2011**, *11*, 9450–9466. [[CrossRef](#)]
58. Altintas, Z. Surface plasmon resonance based sensor for the detection of glycopeptide antibiotics in milk using rationally designed nanoMIPs. *Sci. Rep.* **2018**, *8*, 11222. [[CrossRef](#)] [[PubMed](#)]
59. Helmerhorst, E.; Chandler, D.J.; Nussio, M.; Mamotte, C.D. Real-time and Label-free Bio-sensing of Molecular Interactions by Surface Plasmon Resonance: A Laboratory Medicine Perspective. *Clin. Biochem. Rev.* **2012**, *33*, 161–173. [[PubMed](#)]
60. Agrawal, A.; Cho, S.H.; Zandi, O.; Ghosh, S.; Johns, R.W.; Milliron, D.J. Localized Surface Plasmon Resonance in Semiconductor Nanocrystals. *Chem. Rev.* **2018**, *118*, 3121–3207. [[CrossRef](#)] [[PubMed](#)]
61. Jakhmola, A.; Celentano, M.; Vecchione, R.; Manikas, A.; Battista, E.; Calcagno, V.; Netti, P.A. Self-assembly of gold nanowire networks into gold foams: Production, ultrastructure and applications. *Inorg. Chem. Front.* **2017**, *4*, 1033–1041. [[CrossRef](#)]
62. Zhou, Y.; Ji, Y.; Cao, Z. Recent Advances in Optical Detection of Aminoglycosides. *Appl. Sci.* **2020**, *10*, 6579. [[CrossRef](#)]
63. Xu, N.; Qu, C.; Ma, W.; Xu, L.; Xu, L.; Liu, L.; Kuang, H.; Xu, C. Development and application of one-step ELISA for the detection of neomycin in milk. *Food Agric. Immunol.* **2011**, *22*, 259–269. [[CrossRef](#)]
64. Yue, F.; Li, F.; Kong, Q.; Guo, Y.; Sun, X. Recent advances in aptamer-based sensors for aminoglycoside antibiotics detection and their applications. *Sci. Total Environ.* **2021**, *762*, 143129. [[CrossRef](#)] [[PubMed](#)]
65. Nikolaus, N.; Strehli, B. DNA-Aptamers Binding Aminoglycoside Antibiotics. *Sensors* **2014**, *14*, 3737–3755. [[CrossRef](#)]
66. Yan, S.; Lai, X.; Du, G.; Xiang, Y. Identification of aminoglycoside antibiotics in milk matrix with a colorimetric sensor array and pattern recognition methods. *Anal. Chim. Acta* **2018**, *1034*, 153–160. [[CrossRef](#)]
67. Haasnoot, W.; Stouten, P.; Cazemier, G.; Lommen, A.; Nouws, J.F.; Keukens, H.J. Immunochemical detection of aminoglycosides in milk and kidney. *Analyst* **1999**, *124*, 301–305. [[CrossRef](#)]
68. Nivedhini Iswarya, C.; Kiruba Daniel, S.C.G.; Sivakumar, M. Studies on l-histidine capped Ag and Au nanoparticles for dopamine detection. *Mater. Sci. Eng. C* **2017**, *75*, 393–401. [[CrossRef](#)]

69. Shukla, R.; Nune, S.K.; Chanda, N.; Katti, K.; Mekapothula, S.; Kulkarni, R.R.; Welshons, W.V.; Kannan, R.; Katti, K.V. Soybeans as a phytochemical reservoir for the production and stabilization of biocompatible gold nanoparticles. *Small* **2008**, *4*, 1425–1436. [[CrossRef](#)] [[PubMed](#)]
70. Kim, D.-Y.; Shinde, S.; Ghodake, G. Colorimetric detection of magnesium (II) ions using tryptophan functionalized gold nanoparticles. *Sci. Rep.* **2017**, *7*, 3966. [[CrossRef](#)]
71. Sachi, S.; Ferdous, J.; Sikder, M.H.; Azizul Karim Hussani, S.M. Antibiotic residues in milk: Past, present, and future. *J. Adv. Vet. Anim. Res.* **2019**, *6*, 315–332. [[CrossRef](#)]
72. Tan, H.; Chen, Y. Silver nanoparticle enhanced fluorescence of europium (III) for detection of tetracycline in milk. *Sens. Actuators B Chem.* **2012**, *173*, 262–267. [[CrossRef](#)]
73. Mukha, I.; Vityuk, N.; Severynovska, O.; Eremenko, A.; Smirnova, N. The pH-Dependent Structure and Properties of Au and Ag Nanoparticles Produced by Tryptophan Reduction. *Nanoscale Res. Lett.* **2016**, *11*, 101. [[CrossRef](#)]
74. Kim, D.-Y.; Kim, M.; Shinde, S.; Saratale, R.G.; Sung, J.-S.; Ghodake, G. Temperature Dependent Synthesis of Tryptophan-Functionalized Gold Nanoparticles and Their Application in Imaging Human Neuronal Cells. *ACS Sustain. Chem. Eng.* **2017**, *5*, 7678–7689. [[CrossRef](#)]
75. Guan, J.; Jiang, L.; Li, J.; Yang, W. pH-Dependent Aggregation of Histidine-Functionalized Au Nanoparticles Induced by Fe³⁺ Ions. *J. Phys. Chem. C* **2008**, *112*, 3267–3271. [[CrossRef](#)]
76. Zhang, Y.; Hu, Q.; Paau, M.C.; Xie, S.; Gao, P.; Chan, W.; Choi, M.M.F. Probing Histidine-Stabilized Gold Nanoclusters Product by High-Performance Liquid Chromatography and Mass Spectrometry. *J. Phys. Chem. C* **2013**, *117*, 18697–18708. [[CrossRef](#)]
77. Liu, Z.; Zu, Y.; Fu, Y.; Meng, R.; Guo, S.; Xing, Z.; Tan, S. Hydrothermal synthesis of histidine-functionalized single-crystalline gold nanoparticles and their pH-dependent UV absorption characteristic. *Colloids Surf. B Biointerfaces* **2010**, *76*, 311–316. [[CrossRef](#)]
78. Siva, C.; Iswarya, C.N.; Baraneedharan, P.; Sivakumar, M. L-Cysteine assisted formation of mesh like Ag₂S and Ag₃AuS₂ nanocrystals through hydrogen bonds. *Mater. Lett.* **2014**, *134*, 56–59. [[CrossRef](#)]
79. Barth, A. The infrared absorption of amino acid side chains. *Prog. Biophys. Mol. Biol.* **2000**, *74*, 141–173. [[CrossRef](#)]
80. Liu, Z.; Xing, Z.; Zu, Y.; Tan, S.; Zhao, L.; Zhou, Z.; Sun, T. Synthesis and characterization of L-histidine capped silver nanoparticles. *Mater. Sci. Eng. C* **2012**, *32*, 811–816. [[CrossRef](#)]
81. Alharbi, R.; Irannejad, M.; Yavuz, M. A Short Review on the Role of the Metal-Graphene Hybrid Nanostructure in Promoting the Localized Surface Plasmon Resonance Sensor Performance. *Sensors* **2019**, *19*, 862. [[CrossRef](#)] [[PubMed](#)]
82. Luan, Y.; Wang, N.; Li, C.; Guo, X.; Lu, A. Advances in the Application of Aptamer Biosensors to the Detection of Aminoglycoside Antibiotics. *Antibiotics* **2020**, *9*, 787. [[CrossRef](#)]
83. Caglayan, M.G.; Onur, F. A metal-enhanced fluorescence study of primary amines: Determination of aminoglycosides with europium and gold nanoparticles. *Anal. Methods* **2015**, *7*, 1407–1414. [[CrossRef](#)]
84. Guo, Y.; Zhang, Y.; Shao, H.; Wang, Z.; Wang, X.; Jiang, X. Label-Free Colorimetric Detection of Cadmium Ions in Rice Samples Using Gold Nanoparticles. *Anal. Chem.* **2014**, *86*, 8530–8534. [[CrossRef](#)] [[PubMed](#)]
85. Meienberg, K.; Malinina, T.; Nguyen, Z.; Park, C.S.; Glaser, M.A.; Clark, N.A.; Maclennan, J.E. Nanoparticle Aggregation and Fractal Growth in Fluid Smectic Membranes. *Mol. Cryst. Liq. Cryst.* **2015**, *611*, 14–20. [[CrossRef](#)]
86. Lu, G.; Chen, Q.; Li, Y.; Liu, Y.; Zhang, Y.; Huang, Y.; Zhu, L. Status of antibiotic residues and detection techniques used in Chinese milk: A systematic review based on cross-sectional surveillance data. *Food Res. Int.* **2021**, *147*, 110450. [[CrossRef](#)]
87. Layada, S.; Benouareth, D.-E.; Coucke, W.; Andjelkovic, M. Assessment of antibiotic residues in commercial and farm milk collected in the region of Guelma (Algeria). *Int. J. Food Contam.* **2016**, *3*, 19. [[CrossRef](#)]
88. Rahman, M.S.; Hassan, M.M.; Chowdhury, S. Determination of antibiotic residues in milk and assessment of human health risk in Bangladesh. *Heliyon* **2021**, *7*, e07739. [[CrossRef](#)]
89. Moghadam, M.M.; Amiri, M.; Riabi, H.R.A.; Riabi, H.R.A. Evaluation of Antibiotic Residues in Pasteurized and Raw Milk Distributed in the South of Khorasan-e Razavi Province, Iran. *J. Clin. Diagn. Res. JCDR* **2016**, *10*, FC31–FC35. [[CrossRef](#)] [[PubMed](#)]
90. Chiesa, L.M.; Di Cesare, F.; Nobile, M.; Villa, R.; Decastelli, L.; Martucci, F.; Fontana, M.; Pavlovic, R.; Arioli, F.; Panseri, S. Antibiotics and Non-Targeted Metabolite Residues Detection as a Comprehensive Approach toward Food Safety in Raw Milk. *Foods* **2021**, *10*, 544. [[CrossRef](#)] [[PubMed](#)]
91. Kumar, N.; Sharma, G.; Leahy, E.; Shome, B.R.; Bandyopadhyay, S.; Deka, R.P.; Shome, R.; Dey, T.K.; Lindahl, J.F. Understanding Antibiotic Usage on Small-Scale Dairy Farms in the Indian States of Assam and Haryana Using a Mixed-Methods Approach—Outcomes and Challenges. *Antibiotics* **2021**, *10*, 1124. [[CrossRef](#)] [[PubMed](#)]